Functional Composites and Structures

PAPER

Repetitive heating performance of MgO-activated ground granulated blast furnace slag composites containing MWCNTs

IOP Publishing Funct. Compos. Struct. 3 (2021) 015003 https://doi.org/10.1088/2631-6331/abdd97

Functional Composites and Structures

PAPER

Repetitive heating performance of MgO-activated ground granulated blast furnace slag composites containing MWCNTs

Jinho Bang, Hyeong Min Park and Beomjoo Yang

School of Civil Engineering, Chungbuk National University, 1 Chungdae-ro, Seowon-gu, Cheongju, Chungbuk 28644, Republic of Korea

E-mail: byang@cbnu.ac.kr

RECEIVED
22 December 2020

REVISED
16 January 2021

ACCEPTED FOR PUBLICATION
19 January 2021

PUBLISHED
4 February 2021

Keywords: repetitive heating performance, magnesium oxide, blast furnace slag, multi-walled carbon nanotubes, electrical resistivity

Abstract

Recently, various studies have been conducted in an effort to apply the outstanding properties of nanomaterials to construction fields. The present study aims to investigate the repetitive heating characteristics of magnesium oxide (MgO)-activated slag composites containing multi-walled carbon nanotubes (MWCNTs). MgO-activated slag composites with various mix proportions were fabricated through facile mechanical mixing method and cured at various temperatures. The electrical resistivity and compressive strength of the specimens were measured, and the cyclical heating performance was also analyzed under a constant ampere condition. Microstructural and thermal analyses of the MgO-activated slag composites were carried out by means of a scanning electron microscope and a thermogravimetry analysis, respectively. The content of MWCNTs and the curing conditions affected the overall electrical resistivity, compressive strength, and heat-generation properties of the composites. Here, related mechanisms are addressed in connection with the hydration process of the binder material.

1. Introduction

Along with the progress in industrial technology, the demand for multifunctional high-performance construction materials has increased in the construction field. Carbon nanotube (CNT), known as a representative nano material, has excellent mechanical, electrical, thermal, and physical properties [1–3]. In order to utilize these excellent properties of CNT, various experimental studies of cement composites with CNT have been conducted in the civil engineering field over the last few decades. Specifically, with regard to cementitious composites, energy harvesting, structural health monitoring (SHM), electromagnetic interference (EMI) shielding, and heat generation have been investigated [4–15].

Electrified cementitious composites can be applied to various fields. In previous studies, the piezoresistive energy harvesting and SHM of cementitious composites were reported [4–8]. Nam *et al* and Zhang *et al* reported that the CNT incorporated into cementitious composites offers advantageous potential as an EMI shielding construction material [9–11]. Wei *et al* and Ghosh *et al* reported that electrified cementitious composites with multi-walled carbon nanotubes (MWCNTs) can be used in thermoelectric energy harvesting application in the civil engineering field [12, 13]. Kim *et al* also reported the heat-generation characteristics of MWCNTs-incorporated cement-based composites [14, 15].

However, despite the outstanding advantageous of CNT-incorporated cementitious composites, there remains the significant problem and serious, environmental issue of global warming in relation to cement production. The manufacturing of Portland cement (PC) requires the calcination of limestone at fairy high temperatures and this process is responsible for the generation of 8% of global CO_2 emissions [16–19]. Ground granulated blast furnace slag (GGBS), a by-product of iron production, can be utilized as a partial replacement for PC. Accordingly, research related to GGBS is actively underway.

The chemical and micro structural characteristics as well as, the durability of slag as a binder material are heavily influenced by the properties of the alkali-activator solution used. The activator solution, which is a mixture of water, sodium hydroxide, and sodium silicate, induces a hydration reaction by penetrating the

Table 1. Chemical composition of the GGBS According to x-ray fluorescence (wt.%) [16].

	CaO	SiO_2	Al_2O_3	Fe_2O_3	MgO	Na_2O	K_2O	SO_3	TiO_2	Mn_2O_3	SrO	LOI[a]
Slag	44.8	33.5	13.7	0.5	2.9	0.2	0.5	1.7	0.5	0.2	0.1	1.4

[a] LOI: Limiting oxygen index

Table 2. Mix proportion of specimens.

Specimen	Slag (g)	MgO[a] (g)	MWCNTs (g)	Water (g)	Silica fume (g)	Superplasticizer (g)	Flow (mm)
C0	100	10	—	52	10	1.6	110
C1			1	85			100
C2			2	105			100

[a] MgO: Magnesium oxide

glassy layer on the surface of the slag. However, the conventional method is fairly complex to achieve a proper alkaline concentration level, and it is difficult to control the setting time. Magnesium oxide (MgO) when added to slag induces a reaction similar to that by an alkaline activator, causing the reaction by the removing the glassy surface layer of the slag. The reaction product, which can be calcium aluminate silicate hydrates (C–A–S–H), portlandite, ettringite, and hydrotalcite depending on the content of the MgO, is main factor determining the properties of hardened GGBS. Based on the abovementioned mechanisms, various studies of areas not previously examined are now being carried out.

Jin *et al* studied the hydration of MgO-activated GGBS paste, and discovered that the strength performance of MgO-GGBS blends is affected by the reactivity of the MgO [20]. Yoon *et al* investigated the influence of MgO on the chloride penetration resistance of alkali-activated materials (i.e. fly ash and slag) [21]. Park *et al* reported that a higher MgO content increased the degree of the reaction of slag; they also, investigated the carbonation behavior of alkali-activated slag modified with MgO [22, 23].

Construction composites composed of the MgO-slag binder with MWCNTs are expected to lead to significant changes in the construction industry, though few studies in this area have been reported to date. In particular, there has been no research on the repetitive heating performance of MgO-slag binder containing MWCNTs and the effects on composites. Hence, the present study aims to investigate the repetitive heating properties of MgO-activated slag composites with MWCNTs. MgO-activated slag composites with three different curing conditions and mix proportions were fabricated. The electrical resistivity and compressive strength of the specimens were investigated, and the cyclical heating performance capabilities were also analyzed by applying amperage of 0.3 A to MWCNTs-incorporated MgO-activated slag composites. A microstructural assessment of the MgO-activated slag composite was also conducted by a thermogravimetric analysis (TG/DTG) and scanning electron microscopy (SEM).

2. Experimental procedure

2.1. Materials and specimen preparation

The chemical compositions of the GGBS (Hyundai Steel Co., Ltd, Republic of Korea) used in this study is listed in table 1 [23]. Polycarboxylate superplasticizer (GLENIUM 8008 by BASF Pozzolith Ltd) and silica fume (EMS-970 manufactured by Elkem Inc.) were used as an admixture to enhance the dispersion of the CNT bundles in the cementitious composites and to improve the workability [24], and MgO (Samchun Chemical Co., Ltd, Republic of Korea, light-burned, 96% purity) was included at 10 wt.% according to the amount of slag. MWCNTs (Jeno Tube 8 ©, JEIO Co., Ltd, Republic of Korea) with a purity level of 98.5% was used as an electrically conductive filler. The length and diameter of the MWCNTs were 100–200 μm and 7–9 nm, respectively. Table 2 shows the mix proportion of the present specimens used here.

Three different mix proportions with various contents of MWCNTs were used to manufacture the specimens. The MWCNTs used to prepare the MgO-activated slag composites had three different quantities (0, 1, and 2 wt.%), and for all specimens, silica fume, a superplasticizer, and MgO were fixed at identical amounts. The ratio of the binder material to water was minimized in approximate conformity with the target flow, which was set to 105 $\pm$ 5 mm for all specimens [25]. Each specimen was named according to the content of the MWCNTs and the curing temperature. For example, C2 signifies that 2 wt.% of MWCNTs is contained into the specimen. In addition, C2-60 means that the C2 specimen was cured at 60 °C.

The MgO-activated slag composite specimens with MWCNTs were produced as follows: Slag, MgO, MWCNTs, and silica fume were added to a mixer (HJ-1150, Heungjin Testing Machine Co., Ltd, Republic of

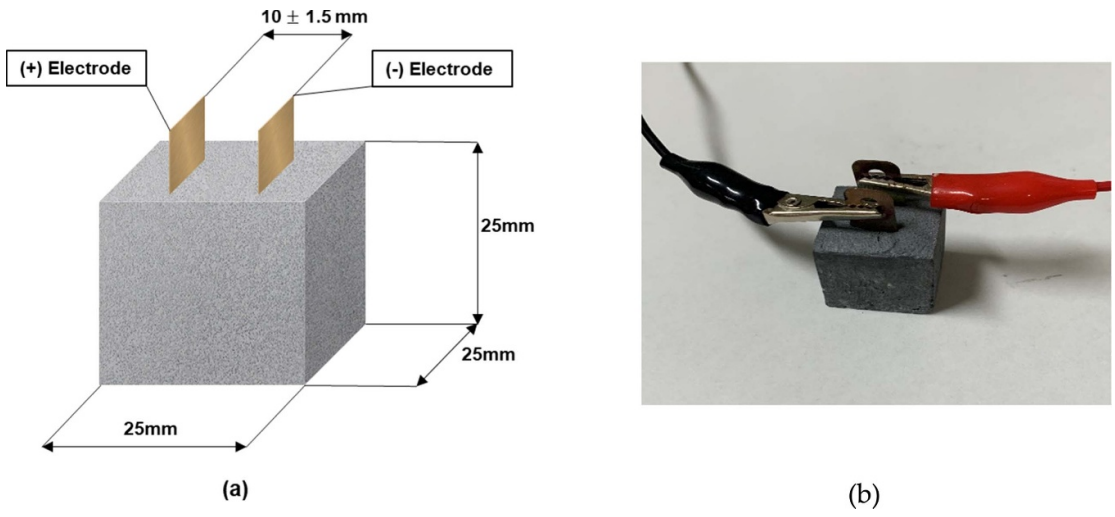

Figure 1. (a) Schematic illustration and (b) test set up of the specimens.

Korea) and mixed for 3 min. A water-containing superplasticizer was then added to the dry mixture and this was mixed for 5 min [26], after which the mixture was poured into a mold. As shown in figure 1(a), the fabricated MgO-activated slag composites were 25 mm × 25 mm × 25 mm in size [3]. Copper with an electrode distance of 10 ± 1.5 mm were embedded in each specimen at an embedding depth of 25 mm. Each specimen was dried at room temperature for 3 d while wrapped. After 3 d, specimens were cured under various conditions for 25 d. In order to determine the optimal curing condition of these specimens, three conditions were established. The first was sealed by wrapping material and curing at room temperature, and the second and third were sealed by wrapping material and curing at 40 °C and 60 °C, respectively, in an oven.

2.2. Test methods

The electrical resistance of the MgO-activated slag composites was determined by the two-probe method. The electrical resistance was measured using a digital multimeter (FLUKE-116, Fluke Co., USA), with the equation bellow.

$$\rho = R \cdot \frac{A}{L}. \tag{1}$$

Here ρ and R correspondingly denote the electrical resistivity and the electrical resistance. Additionally, L and A are the distance between the copper electrodes and the cross-sectional area (mm^2) of the copper electrodes applied to the specimens, respectively [27–29]. A compressive strength test was conducted with a universal testing machine (UTM; HST-200CS, Hanshin Kumpung Inc. Republic of Korea) at 0.01 mm s^{-1} in accordance with ASTM C 109 [30].

The heating performance of the specimens was examined by a cyclic test. The electric current for the heat-generation test was fixed at 0.3 A for all specimens, and an identical level of electric current was applied to all cyclic heating tests. The designated ampere level was forced onto all specimens with a DC power supply (PL-3005S, GS Instech Co., Ltd, Republic of Korea), and the surface temperatures were measured by a thermal imaging infrared camera (FLIR E5 Wifi, FLIR® Systems, Inc. USA). The assigned electric current was input to the specimens for 30 min, after which, the heated specimens were cooled to the ambient temperature for 30 min. The same processes were repeated for ten cycles. The temperatures and voltages used with the specimens were noted at every cycle throughout the cyclic heating test. Figure 1(b) presents the repetitive heating test set up.

A thermal assessment of the composites was conducted through a thermo-gravimetric (TG) analysis (TGA Q50, TA instruments, USA) of the powder of the specimen. The heating rate was set to 10°C min^{-1} between 30 °C and 800 °C in a nitrogen (N_2) environment. In addition, the morphological characteristics of the specimens were investigated by scanning electron microscopy (SEM; Ultra Plus, ZEISS, Germany). The dispersion degree of the MWCNT fillers in the specimen was also evaluated through SEM analysis. The electricity was conducted through a platinum coating to the specimen for an accurate SEM analysis.

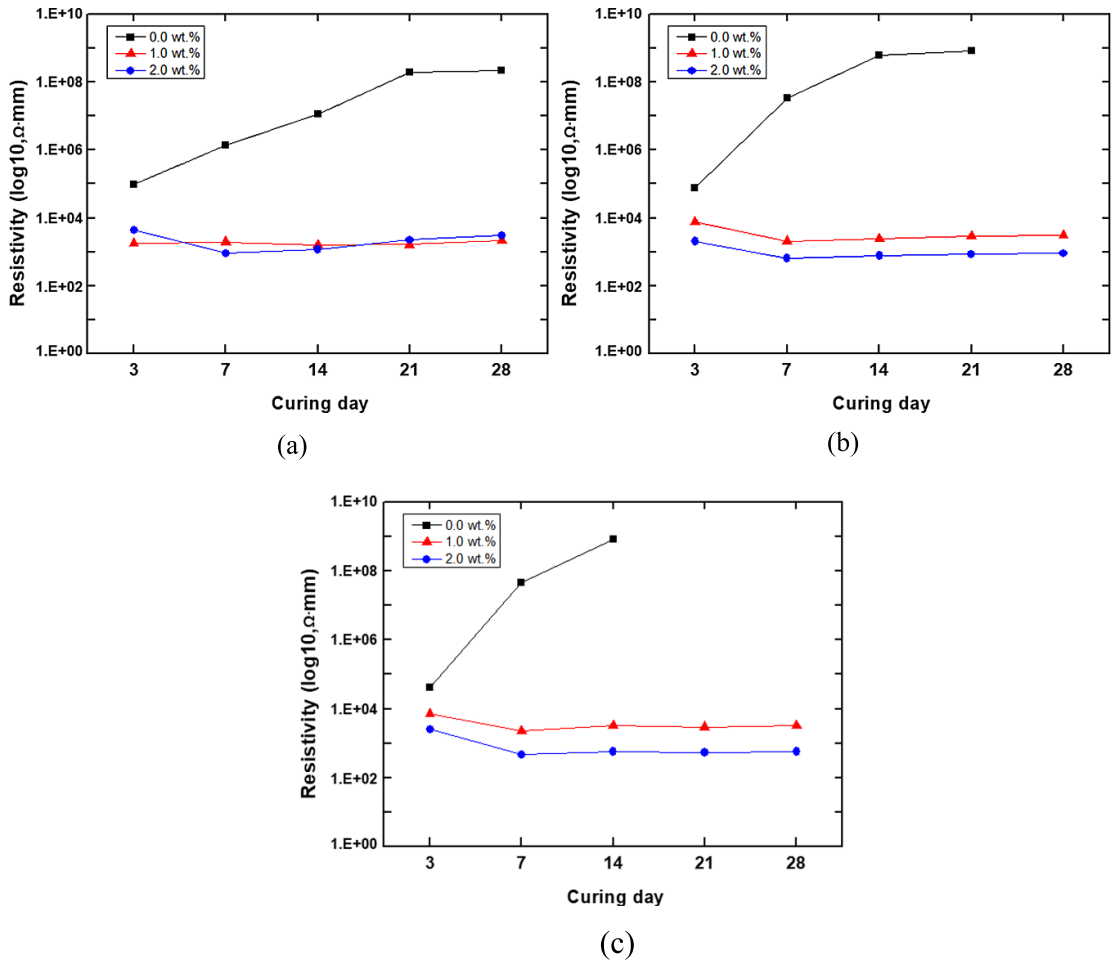

Figure 2. Electrical resistivity according to the number of curing days for different hardening conditions: (a) room temperature, (b) 40 °C oven drying, and (c) 60 °C oven drying.

3. Results and discussion

3.1. Electrical resistivity

Figure 2 presents the electric resistivity of the MgO-activated slag composites over a period of 28 days. In all curing conditions, the electric resistivity of the specimens without MWCNT (C0) increased as curing proceeded. The rate of increase in the electric resistivity varied according to the MWCNT content.
The electric resistivity of the specimen cured at room temperature increased relatively slowly compared to the specimens cured in an oven at 40 °C and 60 °C. In the oven-cured specimens, the increase rate of resistivity was very high from the beginning, and the resistivity of the specimen cured at 40 °C and 60 °C (C-40 and C-60) were too high to be measured after 21 and 14 days, respectively. This outcome is attributed to the rapid evaporation of the water molecules that maintain the conductivity in the composites and to the accelerated formation of hydrates due to the oven curing step.

In the specimens containing MWCNTs (C1 and C2), the electrical resistivity tended to be maintained or to decrease from the initial stage according to the curing progress used. This occurred due to the formation of an internal conductive network caused by the MWCNT, and a lower resistivity value was measured when more of the MWCNTs were incorporated into the binder. The evaporation of water molecules and the promotion of hydration under the oven curing condition works equally well for composites containing MWCNTs. However, this approach is advantageous to lower the effective resistivity of the composites by forming a more stable conductive path composed of MWCNT with relatively high electrical conductivity.

Figure 3 shows the normalized electrical resistivity according to the curing conditions and MWCNT contents. The overall trend is similar to that of the resistivity values. Figure3 more clearly indicates the difference in the electric resistivity value after seven days at various curing temperatures. Among the specimens containing MWCNTs in the room temperature condition, C1 showed similar electrical resistivity from 3 to 28 d of curing; however, in C2, the electrical resistivity decreased by 80% and then increased with

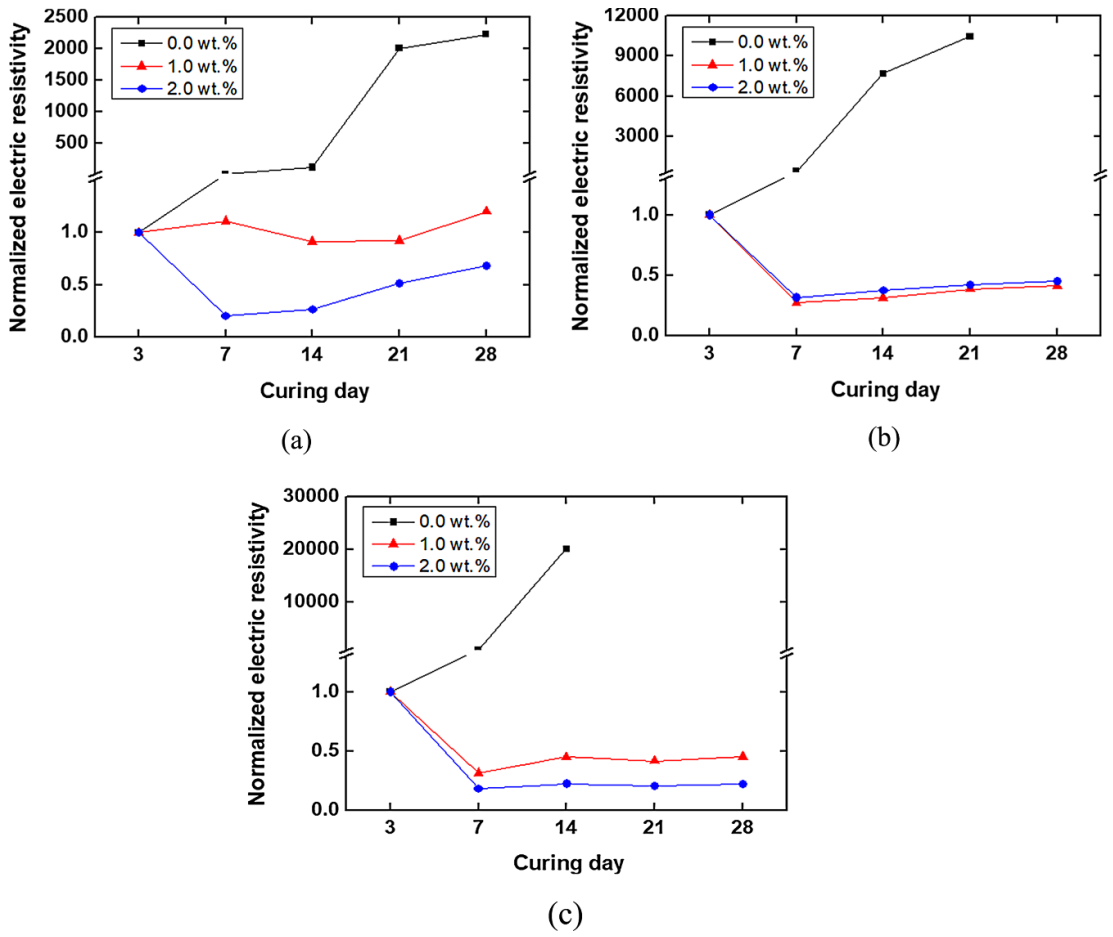

Figure 3. Normalized electric resistivity after several curing days for various hardening conditions: (a) room temperature, (b) 40 °C oven drying, and (c) 60 °C oven drying.

time, as shown in figure 3(a). On the other hand, as shown in figures 3(b) and (c), the electric resistivity of C-40 and C-60 decreased after 3 d of curing and then remained stable; however, this was not noted in C0.

It is presumed that the curing temperature affected the hydration rate of the binder material, resulting in a change in the resistivity. In other words, when hardening of the binder material mixed with MWCNTs is not sufficiently conducted, the internal nano structure easily deforms as the hydration proceeds. However, the ideal curing temperature helps to stabilize the conductive paths which form initially; thus, the electrical resistivity value of the specimen remains. The decreased electrical resistivity outcomes of C-40 and C-60 with MWCNTs are due to the reduction of voids inside the specimen. At room temperature, the moisture which filled in the voids evaporates over time, exiting through the capillary tubes. Curing at a high temperature, however, promotes a reaction with the surrounding binders, leading to the formation of hydrates and to a reduction in the effective resistivity.

3.2. Compressive strength

Figure 4 shows the compressive strength of the MgO-activated slag composites after curing for 28 days. The compressive strength tests were carried out using specimens before the heat-generation test. Curing under conditions above room temperature helped to improve the compressive strength of the composites. In particular, C0-60 showed the highest compressive strength. As in the case of the electrical resistivity, it is presumed that the high temperature accelerated the hydration of the alkali-activated binder material. When the curing temperature exceeds room temperature, it is expected that the hydration of the composite is accelerated, and early strength is signified.

On the other hand, it was observed that the compressive strength decreased as the amount of incorporated MWCNTs was increased. Specifically, the compressive strength of the specimens containing 1 and 2 wt.% of MWCNTs decreased by approximately 38% and 43%, respectively. For the C1 and C2 specimens, MWCNT produces a weak connection between the hydration products of the composites and decreases the compressive strength of the composites. In addition, when excess MWCNT is added to the mix

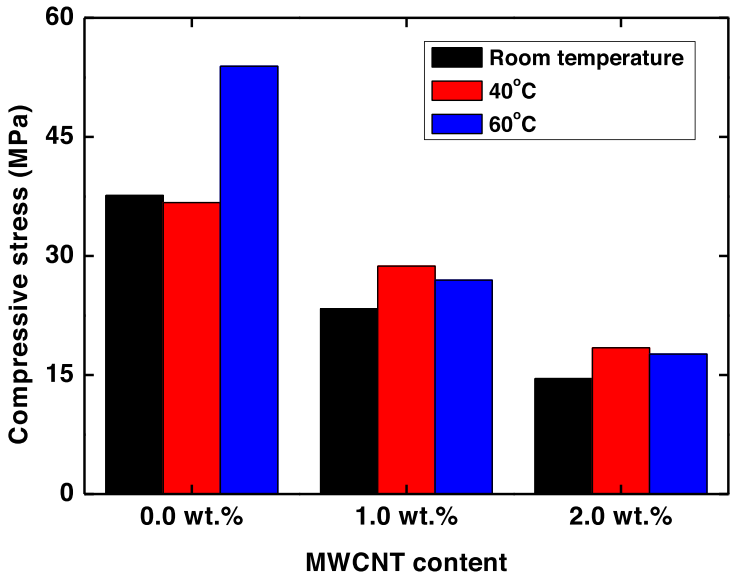

Figure 4. Compressive strength of MgO-activated slag composites incorporating MWCNTs.

(C2), agglomeration of the MWCNT is prevalent, during which proper dispersion of the electric filler is not achieved. The agglomeration creates voids that hinder any improvement in the mechanical properties of the composites, ultimately causing a decrease in the compressive strength.

The experimental results conducted in this study are similar to the literature that studies the effect of dispersion of MWCNTs in slag-based composites. Khater *et al* provided experimental insights on the correlation between the amount of MWCNTs and the compressive strength of the slag composites [31]. It was revealed by [31] that the appropriate amount of MWCNTs to improve the compressive strength of the slag composites was 0.1–0.4 wt.%; however, it was also found that the incorporation of MWCNTs more than 0.4 wt.% resulted in a decrease in compressive strength due to agglomeration of MWCNTs and an increase in voids [31]. Furthermore, it was reported in additional previous studies that excessive incorporation of MWCNTs causes agglomeration of the fillers in the slag binder and decreases in compressive strength of composites [32, 33]. In the present study, we focused on electrical resistivity and repetitive heating performance rather than compressive strength of composites, and thus the amount of MWCNTs was set at 1–2 wt.%, which is higher than those of existing literatures.

3.3. Repetitive heating performance

Figure 5 shows the temperature, ampere, voltage, and cycling history of the MWCNT-incorporated MgO-activated slag composites. A summary of the heating performance results is also presented in figure 6. The heating phenomenon by the inputted ampere for the composites was ascribed to the electrically conductive network caused by the MWCNTs dispersed in the matrix. The heat temperature generated by the amperage applied to the specimen was slightly increased with elevated cycling, as shown in figures 6(a) and (b). In the C1 case, the temperature was higher by approximately 20 °C than that of C2. On the other hand, as shown in figures 6(c) and (d), there were almost no temperature fluctuations even when elevated cycling took place. The heating performance of C1 was much better than that of C2.

Overall, the heat-generation performance was better for C1 than for C2, and C-60 was better than C-40. This presumably arises because 1 wt.% of MWCNT is more suitable for forming optimal conductive paths to cause Joule heating in a cementitious matrix environment. In addition, it is believed that the more stable heat-generation performance of C-60 is due to the development of high mechanical properties stemming from the rapid hydration. As a result, the deformation of the internal conductive paths due to heat generation is reduced, and higher resistance to microcracks is thus obtained.

Figure 7 shows thermal images of MgO-activated slag composites with different amounts of the electrically conductive filler after 30 min of heating. Although the thermal images were taken at the same time, it can be seen that C1 exhibits higher heating performance than C2. For C1 (figure 7(a)), the heat was generated relatively evenly, whereas for C2 (figure 7(b)), the heat was concentrated in the upper center of the specimen. These various characteristics of the MWCNT-incorporated MgO-activated slag composites evaluated here are summarized in table 3.

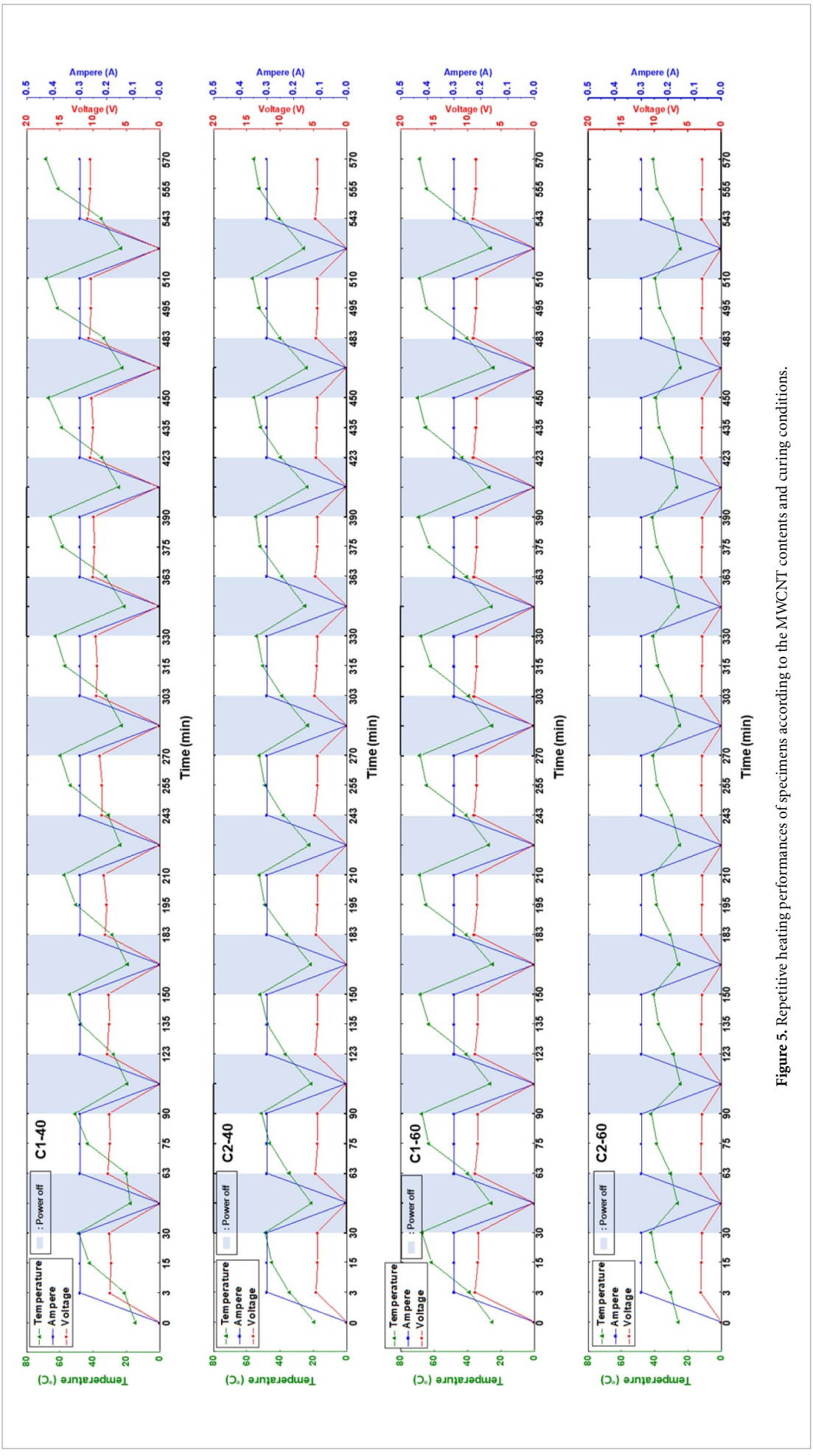

Figure 5. Repetitive heating performances of specimens according to the MWCNT contents and curing conditions.

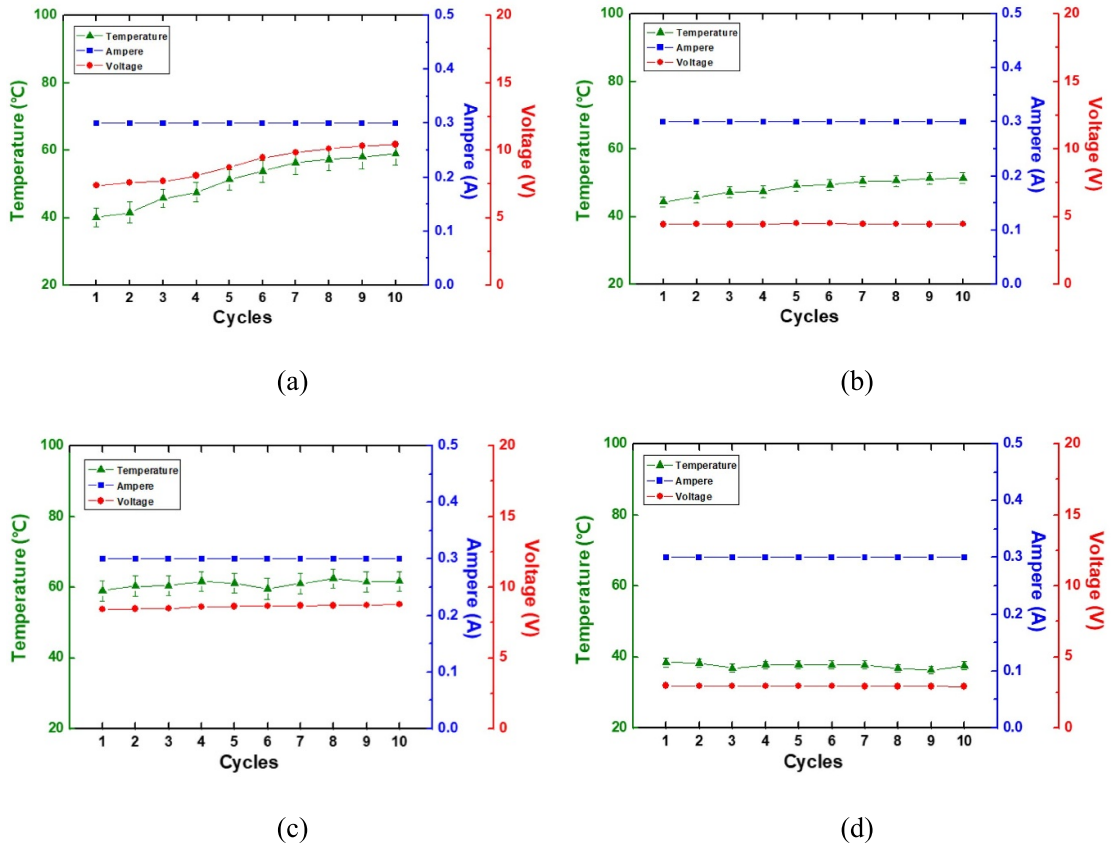

Figure 6. Summary of the heating performance outcomes of MWCNT-incorporated MgO-slag composites: (a) C1-40, (b) C2-40, (c) C1-60, and (d) C2-60.

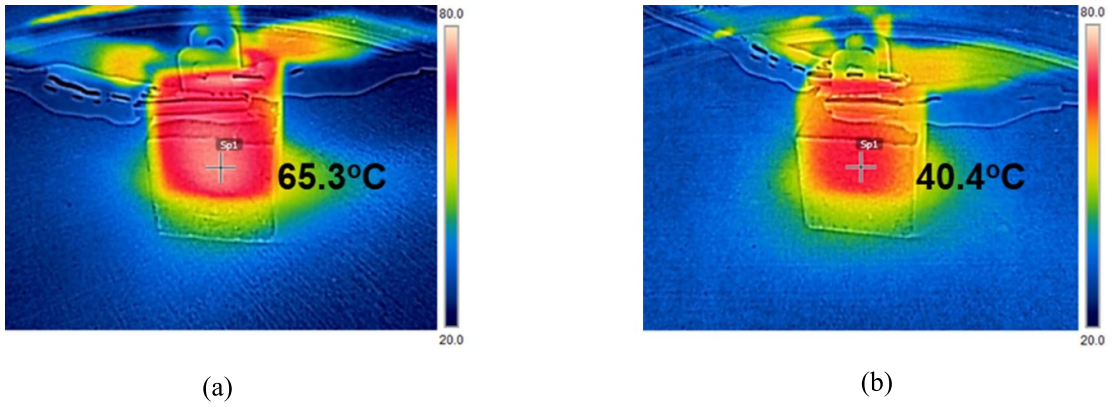

Figure 7. Thermal images of the MgO-activated slag composites (a) C1-60, and (b) C2-60.

3.4. SEM and thermal analyses

SEM micrograph images of MgO-activated slag composites at various mix proportions and under curing conditions are presented in figure 8. Figures 8(a)—(d) show SEM images of the C0-R, C0-40, C1-R, and C1-40 specimens, respectively. C–A–S–H is apparent in figures 8(a) and (b) as the representative hydrate products of MgO-activated slag composites [34]. It was difficult to find differences in the slag-based matrix morphologies according to the curing condition. On the other hand, at amounts beyond the percolation threshold of MWCNT, such as MWCNT amounts exceeding 1 wt.%, agglomeration was detected regardless of the curing condition. Figure 8(c) and (d) depict MWCNT agglomeration in the C1-R and C1-40 specimens, respectively [35–37]. An excessive amount of MWCNT disturbed the consistent dispersion of the

Table 3. Characteristics of the present specimens: resistivity, compressive strength, heat-generating temperature, and voltage.

Specimen	Resistivity ($\log_{10}$, Ω mm, 28 d)	Compressive strength (MPa)	Maximum generating temperature (°C, max)	Voltage (V, max) (input 0.3 A)
C0-R	8.33	37.63	—	—
C1-R	3.33	23.36	—	—
C2-R	3.48	14.56	—	—
C0-40	—	33.79	—	—
C1-40	3.49	28.72	58.96	10.45
C2-40	2.96	14.21	51.44	4.49
C0-60	—	53.92	—	—
C1-60	3.51	26.96	62.45	8.78
C2-60	2.75	17.63	38.41	2.91

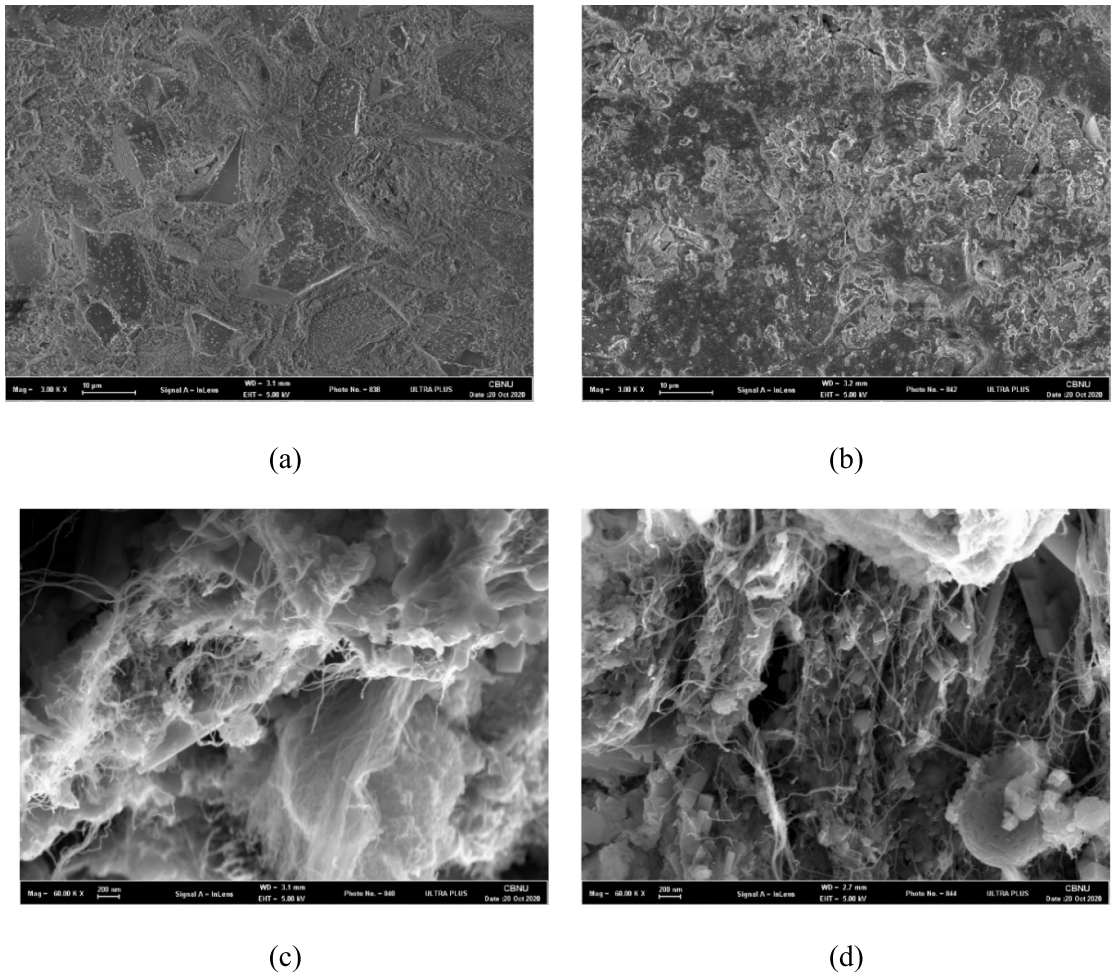

Figure 8. SEM micrographs of the (a) C0-R, (b) C0-40, (c) C1-R, and (d) C1-40 specimens.

MWCNT in the composites, inducing agglomeration of the electrical filler materials. In addition, numerous micropores were observed in the aggregates of MWCNT, specifically in the internal structure [38].

TG and the derivative of TG (DTG) peaks of the MgO-activated slag composites are presented in figure 9. The first phase involves a decrease in the mass of the MgO-activated slag composite specimens in the temperature range of 90–100 °C due to the evaporation of the bound water from the C–S–H and possibly the M–S–H types of gels. Temperatures ranging from 350 to 400 °C on the DTG curves may be where the decomposition of hydrotalcite-like phases (Ht) mainly occurs. In that range, brucite and Ht phases may exist depending on the degree of the hydrate reaction between the slag and the MgO. It is difficult to distinguish a specific phase only using a TG/DTG analysis as performed in this study. However, earlier work reported that no brucite was found after a XRD analysis of MgO-activated slag composites cured at room temperature

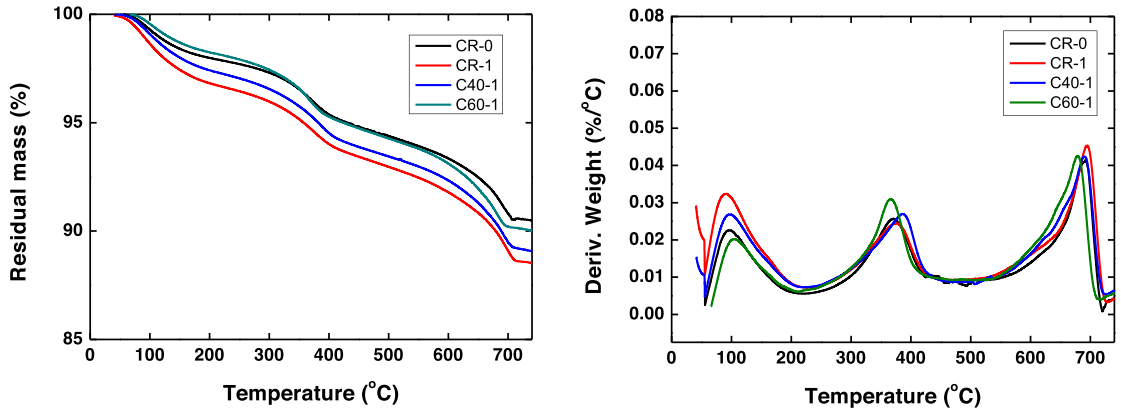

Figure 9. TGA of MgO slag composites: (a) TG and (b) DTG.

[20, 39]. Hence, in this study, it is considered that the Ht phase formed more prevalently than the brucite phase, in which a relatively large amount of MgO and high-temperature curing conditions were considered. At the temperature range of 650–700 °C, the third hump includes the decomposition of various carbonate-containing phases, including calcite, magnesium carbonate, and Ht induced from the carbonation of the raw material.

4. Conclusions

The repetitive heating performance capabilities of MWCNT-incorporated MgO-activated slag composites according to the MWCNT content and curing condition were investigated and analyzed in the present study. The electrical resistivity, compressive strength, and cyclic heat-generation performance outcomes of the composites were measured. In addition, microstructural and thermal analyses of the MgO-activated slag composites were carried out via SEM and TG/DTG, respectively. The findings here are summarized below.

- The content of MWCNT and the curing temperature had considerable effect on the overall performances of the specimens. In terms of electrical resistivity, a high MWCNT content was helpful; however, 1 wt.% was ideal considering the compressive strength and heat-generation performance.
- A curing temperature higher than room temperature (40 °C and 60 °C) had positive effects on the electrical resistivity, compressive strength, and heat-generation performances of the specimens. According to the results of heat performance tests, for C-40 it was observed that temperature fluctuations occurred as the heating cycle was repeated. On the other hand, C-60 exhibited more stable heat-generation performance.
- The electrical resistivity of C0 increased with longer curing times. On the other hand, regardless of the curing condition, the electrical resistivity outcomes of the C1 and C2 specimens were significantly lower than that of C0, though the resistivity remained constant over time.
- For the results of compressive strength tests, the C0-60 specimen showed the highest value. Increasing the MWCNT content decreased the compressive strength, indicating that the addition of an electrical nanofiller may negatively affect the hydration reaction.

Repetitive heating performance capabilities of MgO-activated slag composites containing MWNCT, as tested here, have not been previously reported. Therefore, comparison with earlier work were challenging. Overall, in this study, mixed data from the experimental results of slag-based composites, cementitious composites containing MWCNTs, and self-heating construction materials were observed. Deeper considerations are necessary for a more thorough analysis of these results. While, such analyses are beyond the scope of the present study, more detailed studies are planned for the near future.

Acknowledgments

This study was supported by a grant from National Research Foundation of Korea (NRF) funded by the Korea government (MSIT) (2020R1C1C1005063). In addition, following are results of a study on the

'Leaders in INdustry-university Cooperation +' Project, supported by the Ministry of Education and National Research Foundation of Korea (1345323364).

ORCID iD

Beomjoo Yang https://orcid.org/0000-0002-2675-9774

References

[1] Alkhateb H, Al-Ostaz A, Cheng A H D and Li X 2013 Materials genome for graphene-cement nanocomposites *J. Nanomater. Micromech.* **3** 67–77
[2] Al-Dahawi A, Öztürk O, Emami F, Yıldırım G and Şahmaran M 2016 Effect of mixing methods on the electrical properties of cementitious composites incorporating different carbon-based materials *Constr. Build. Mater.* **104** 160–8
[3] Al-Dahawi A, Sarwary M H, Öztürk O, Yıldırım G, Akın A, Şahmaran M and Lachemi M 2016 Electrical percolation threshold of cementitious composites possessing self-sensing functionality incorporating different carbon-based materials *Smart Mater. Struct.* **25** 105005
[4] Han B, Zhang K, Yu X, Kwon E and Ou J 2012 Electrical characteristics and pressure-sensitive response measurements of carboxyl MWNT/cement composites *Cem. Concr. Compos.* **34** 794–800
[5] Kim H K, Park I S and Lee H K 2014 Improved piezoresistive sensitivity and stability of CNT/cement mortar composites with low water–binder ratio *Compos. Struct.* **116** 713–9
[6] Kim G M, Yang B J, Ryu G U and Lee H K 2016 The electrically conductive carbon nanotube (CNT)/cement composites for accelerated curing and thermal cracking reduction *Compos. Struct.* **158** 20–29
[7] Yang F and Qian S 2020 Mechanical and piezoelectric properties of ECC with CNT incorporated through fiber modification *Constr. Build. Mater.* **260** 119717
[8] Dong W, Li W, Wang K, Guo Y, Sheng D and Shah S P 2020 Piezoresistivity enhancement of functional carbon black filled cement-based sensor using polypropylene fibre *Powder Technol.* **373** 184–94
[9] Nam I W, Lee H K and Jang J H 2011 Electromagnetic interference shielding/absorbing characteristics of CNT-embedded epoxy composites *Composites* A **42** 1110–8
[10] Nam I W, Kim H K and Lee H K 2012 Influence of silica fume additions on electromagnetic interference shielding effectiveness of multi-walled carbon nanotube/cement composites *Constr. Build. Mater.* **30** 480–7
[11] Zhang L, Li L, Wang Y, Yu X and Han B 2020 Multifunctional cement-based materials modified with electrostatic self-assembled CNT/TiO_2 composite filler *Constr. Build. Mater.* **238** 117787
[12] Ghosh S, Harish S, Ohtaki M and Saha B B 2020 Enhanced figure of merit of cement composites with graphene and ZnO nanoinclusions for efficient energy harvesting in buildings *Energy* **198** 117396
[13] Wei J, Zhang M, Wang Y, Qiao S, Zhang H and Li X 2020 Synergistic optimization of thermoelectric performance in cementitious composites by lithium carbonate and carbon nanotubes *Int. J. Energy Res.* **45** 2460-2473
[14] Kim G M, Naeem F, Kim H K and Lee H K 2016 Heating and heat-dependent mechanical characteristics of CNT-embedded cementitious composites *Compos. Struct.* **136** 162–70
[15] Kim G M, Yang B J, Yoon H N and Lee H K 2018 Synergistic effects of carbon nanotubes and carbon fibers on heat generation and electrical characteristics of cementitious composites *Carbon* **134** 283–92
[16] Hewlett P and Liska M 2019 *Lea's Chemistry of Cement and Concrete* 5th edn (London: Butterworth-Heinemann)
[17] Malhotra V M 2002 Introduction: sustainable development and concrete technology *Concr. Int.* **24** 22
[18] Mehta P K 2001 Reducing the environmental impact of concrete *Concr. Int.* **23** 61–66
[19] Fairbairn E M, Americano B B, Cordeiro G C, Paula T P, Toledo Filho R D and Silvoso M M 2010 Cement replacement by sugar cane bagasse ash: CO_2 emissions reduction and potential for carbon credits *J. Environ. Manage.* **91** 1864–71
[20] Jin F, Gu K and Al-Tabbaa A 2015 Strength and hydration properties of reactive MgO-activated ground granulated blastfurnace slag paste *Cem. Concr. Compos.* **57** 8–16
[21] Yoon H N, Park S M and Lee H K 2018 Effect of MgO on chloride penetration resistance of alkali-activated binder *Constr. Build. Mater.* **178** 584–92
[22] Park S M, Jang J G and Lee H K 2018 Unlocking the role of MgO in the carbonation of alkali-activated slag cement *Inorg. Chem. Front.* **5** 1661–70
[23] Park S, Park H M, Yoon H N, Seo J, Yang C M, Provis J L and Yang B 2020 Hydration kinetics and products of MgO-activated blast furnace slag *Constr. Build. Mater.* **249** 118700
[24] Kim G M, Nam I W, Yoon H N and Lee H K 2018 Effect of superplasticizer type and siliceous materials on the dispersion of carbon nanotube in cementitious composites *Compos. Struct.* **185** 264–72
[25] Nam I W and Lee H K 2015 Image analysis and DC conductivity measurement for the evaluation of carbon nanotube distribution in cement matrix *Int. J. Concr. Struct. Mater.* **9** 427–38
[26] Kim G M, Kim Y K, Kim Y J, Seo J H, Yang B J and Lee H K 2019 Enhancement of the modulus of compression of calcium silicate hydrates via covalent synthesis of CNT and silica fume *Constr. Build. Mater.* **198** 218–25
[27] Park J-M, Kim P-G, Jang J-H, Wang Z, Kim J-W, Lee W-I, Park J-G and DeVries K L 2008 Self-sensing and dispersive evaluation of single carbon fiber/carbon nanotube (CNT)-epoxy composites using electro-micromechanical technique and nondestructive acoustic emission *Composites* B **39** 1170–82
[28] Park H M, Kim G M, Lee S Y, Jeon H, Kim S Y, Kim M, Kim J W, Jung Y C and Yang B J 2018 Electrical resistivity reduction with pitch-based carbon fiber into multi-walled carbon nanotube (MWCNT)-embedded cement composites *Constr. Build. Mater.* **165** 484–93
[29] Park H M, Park S M, Lee S M, Shon I J, Jeon H and Yang B J 2019 Automated generation of carbon nanotube morphology in cement composite via data-driven approaches emission *Composites* B **167** 51–62
[30] ASTM C109 2005 Standard test method for compressive strength of hydraulic cement mortars (using 2-in. [50 mm] cube specimens) (West Conshohocken, PA: American Society of Testing and Materials)
[31] Khater H M and Abd El Gawaad H A 2016 Characterization of alkali activated geopolymer mortar doped with MWCNT *Constr. Build. Mater.* **102** 329–37

[32] Rovnaník P, Šimonová H, Topolář L, Bayer P, Schmid P and Keršner Z 2016 Carbon nanotube reinforced alkali-activated slag mortars *Constr. Build. Mater.* **119** 223–9
[33] Park H M, Park C, Bang J, Lee M and Yang B 2020 Synergistic effect of MWCNT and carbon fiber hybrid fillers on electrical and mechanical properties of alkali-activated slag composites *Crystals* **10** 1139
[34] Ke X, Bernal S A and Provis J L 2016 Controlling the reaction kinetics of sodium carbonate-activated slag cements using calcined layered double hydroxides *Cem. Concr. Res.* **81** 24–37
[35] Yang B J, Cho K J, Kim G M and Lee H K 2014 Effect of CNT agglomeration on the electrical conductivity and percolation threshold of nanocomposites: a micromechanics-based approach *CMES-Comput. Model. Eng. Sci.* **103** 343–65
[36] Kim S Y, Jang J U, Haile B F, Lee M W and Yang B 2020 Swarm intelligence integrated micromechanical model to investigate thermal conductivity of multi-walled carbon nanotube-embedded cyclic butylene terephthalate thermoplastic nanocomposites *Composites* A **128** 105646
[37] Yang B J, Souri H, Kim S, Ryu S and Lee H K 2014 An analytical model to predict curvature effects of the carbon nanotube on the overall behavior of nanocomposites *J. Appl. Phys.* **116** 033511
[38] Kim G M, Nam I W, Yang B, Yoon H N, Lee H K and Park S 2019 Carbon nanotube (CNT) incorporated cementitious composites for functional construction materials: the state of the art *Compos. Struct.* **227** 111244
[39] Hwang C L, Vo D H, Tran V A and Yehualaw M D 2018 Effect of high MgO content on the performance of alkali-activated fine slag under water and air curing conditions *Constr. Build. Mater.* **186** 503–13